BIOCHEMISTRY
including biophysical chemistry & molecular biology
Rapid Report

Biochemistry **2010,** *49,* 249–251 249
DOI: 10.1021/bi902007b

A Short, Strong Hydrogen Bond in the Active Site of Human Carbonic Anhydrase II[†,‡]

Balendu Sankara Avvaru,[§] Chae Un Kim,[⊥] Katherine H. Sippel,[§] Sol M. Gruner,[⊥,@] Mavis Agbandje-McKenna,[§] David N. Silverman,*[,§,∥] and Robert McKenna*[,§]

[§]*Department of Biochemistry and Molecular Biology,* [∥]*Department of Pharmacology and Therapeutics, College of Medicine, University of Florida, Gainesville, Florida 32610,* [⊥]*Cornell High Energy Synchrotron Source (CHESS), and* [@]*Physics Department, Cornell University, Ithaca, New York 14853*

Received November 23, 2009; Revised Manuscript Received December 9, 2009

ABSTRACT: The crystal structure of human carbonic anhydrase II (HCA II) obtained at 0.9 Å resolution reveals that a water molecule, termed deep water, Dw, and bound in a hydrophobic pocket of the active site forms a short, strong hydrogen bond with the zinc-bound solvent molecule, a conclusion based on the observed oxygen−oxygen distance of 2.45 Å. This water structure has similarities with hydrated hydroxide found in crystals of certain inorganic complexes. The energy required to displace Dw contributes in significant part to the weak binding of CO_2 in the enzyme−substrate complex, a weak binding that enhances k_{cat} for the conversion of CO_2 into bicarbonate. In addition, this short, strong hydrogen bond is expected to contribute to the low pK_a of the zinc-bound water and to promote proton transfer in catalysis.

The hydration of CO_2 to produce bicarbonate and a proton is catalyzed by the carbonic anhydrases (CAs) and plays a significant role in a number of physiological processes, including respiration, fluid secretion, and pH control. There are 14 human gene products classified as CAs, including HCA II which is widespread in tissues and heavily concentrated in red cells. The most efficient of these enzymes, including HCA II, proceed near diffusion control with a k_{cat}/K_m for hydration of 10^8 M^{-1} s^{-1} (*1*, *2*).

Our understanding of the steps in this catalysis is based in significant part on the structure of the active site revealed by X-ray crystallography studies. The first HCA II structures were determined to 2.0 Å resolution and identified the key features of the enzyme mechanism (*3*), whereas subsequent structures obtained between 2.3 and 1.1 Å resolution have focused on a detailed understanding of the geometry about the zinc, orientations of the proton shuttle residue His64, and solvation of residues of the active site (*4*−*6*). Recent structural analysis of HCA II at 0.9 Å resolution reported here allows enhanced interpretation with application to understanding the catalytic mechanism, in particular additional understanding of the role of solvent.

The active site cavity of HCA II is conical and 15 Å deep, having one side lined with predominantly hydrophobic residues and the other lined with hydrophilic residues. At the bottom of the cavity is a zinc ion coordinated in a tetrahedral geometry to three histidine residues (His94, -96, and -119) and a solvent ligand (Figure 1). A wide body of spectroscopic and kinetic data are consistent with a pK_a near 7 describing the protolysis of the aqueous ligand of the metal forming zinc-bound hydroxide (*1*, *2*). The mechanism of catalysis comprises nucleophilic attack of the zinc-bound hydroxide on CO_2, followed by transfer of a proton from zinc-bound water to solution to regenerate the active form (Figure 2). A network of apparently hydrogen bonded water molecules is observed in crystal structures extending from the zinc-bound solvent to the inwardly oriented proton shuttle residue His64 located ~8 Å from the metal (*4*, *5*). This structure of ordered water molecules is likely closely related to viable pathways of proton transfer during catalysis (*7*, *8*).

The final refined 0.9 Å resolution model, 258 residues and 486 water molecules, was refined to an R_{cryst} of 12.5% and an R_{free} of 13.1%. A full description of the structure determination and data collection, and refinement statistics is given in Table S1 (Supporting Information).

Of particular interest for this report is the structure of the apparently hydrogen bonded solvent water network that includes the zinc-bound solvent. This network emanates from the deep water (Dw) in the hydrophobic pocket formed in part by the side chains of Val121, Val143, Trp209, and Leu198 to the water molecules labeled W1, W2, W3a, W3b, and W4 shown in Figures 1, 2, and 3. In crystal structures, this chain extends to but is not in hydrogen bond contact with the proton shuttle residue His64. The zinc-bound solvent appears to form a hydrogen bond with the side chain of Thr199, and the deep water molecule (Dw) appears to participate in hydrogen bonds with the backbone amide of Thr199 and with the zinc-bound water molecule. The mechanism of the proton transfer utilizing pathways such as this has been the subject of considerable investigation (*2*, *7*−*12*).

The current high-resolution structure provides a clearer view of the solvation at the active site (Figure 1). The hydrogen bonds in this water network have distances typical of solvent water, with O−O distances near 2.7−2.9 Å. A more detailed picture of distances and bond angles involving active site solvent is provided in Figures S1 and S2 (Supporting Information). However, there is a short hydrogen bond with an O−O distance estimated to be 2.45 ± 0.03 Å between Dw and the zinc-bound solvent (Figure 3). The crystallographic occupancy is near 100% for Dw, and both this water molecule and the zinc-bound solvent have *B* factors that are low (near 10 $Å^2$) and close in value to the *B* factors of the

[†]This work was funded by grants from the National Institutes of Health (NIH) (Grant GM25154 D.N.S. and R.M.) and the Thomas Maren Foundation (R.M.), the MacCHESS grant (NIH Grant RR001646), U.S. Department of Energy Grant DE-FG02-97ER62443, and CHESS, which is supported by the National Science Foundation (NSF) and the National Institute of General Medical Sciences through NSF Grant DMR-0225180.

[‡]Coordinates are deposited in the Protein Data Bank with accession code 3KS3.

*To whom correspondence should be addressed. D.N.S.: e-mail, silvrmn@ufl.edu; telephone, (352) 392-3556; fax, (352) 392-9696. R.M.: e-mail, rmckenna@ufl.edu; telephone, (352) 392-5695; fax, (352) 392-3422.

Published on Web 12/09/2009

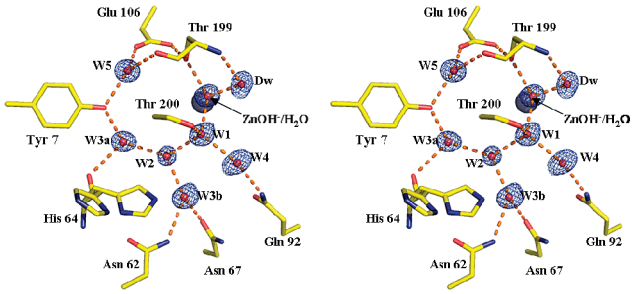

FIGURE 1: Stereoview of the active site of HCA II. The zinc is represented by a gray sphere and the oxygen atoms of water molecules as smaller red spheres. Dotted lines are presumed hydrogen bonds. Stick figures are selected amino acids of the active site with both the inward and outward orientations of His64 shown. The electron density $2F_o - F_c$ Fourier map is contoured at 2.0σ. This figure was created using PyMOL (*28*).

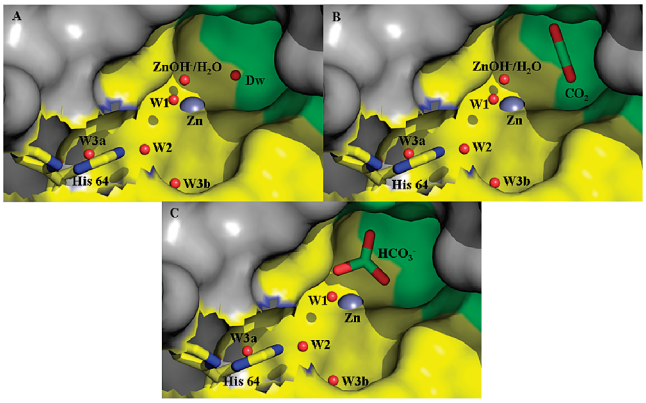

FIGURE 2: Catalytic mechanism: (A) the active site without bound CO_2 showing the deep water, (B) the active site showing bound CO_2 occupying the site of the deep water, and (C) the binding of bicarbonate at the active site of T200H HCA II (*23*). Surface and stick representation: water molecules depicted as red spheres, the hydrophobic residues depicted as green shaded regions, and hydrophilic residues depicted as yellow regions. This figure was created using PyMOL (*28*).

surrounding amino acids. Analysis of the anisotropic thermal motions of Dw indicates that the bulk of its movement is perpendicular to the hydrogen bond with the zinc-bound solvent (Table of Contents Graphic).

Under specific and well-described conditions, short hydrogen bonds involving water with O−O distances of ~2.4 Å have been observed (*13*). These are designated low-barrier hydrogen bonds (LBHBs) reflecting the low barrier for hydrogen movement between the heteroatoms. Such LBHBs are usually observed in nonprotic solvents and involve closely matched values of pK_a for the heteroatoms of the hydrogen bond (*13*).

The Dw is bound in a hydrophobic pocket of the active site. Moreover, with a solution pK_a near 7.0, the zinc-bound solvent in the crystal structure is probably in large part zinc-bound hydroxide under the conditions of crystallization (pH 7.0) (*14*). This structure has similarities with the identification by crystallography of the LBHB of the hydrated hydroxide anion $HOHOH^-$ formed in the hydrophobic region between sheets of phenyl rings in trimethylammonium salts of tris(thiobenzohydroximato)chromate-(III) (*15*). In this case, the O−O atom distance is 2.3 Å in a structure the authors describe as a central proton surrounded by two OH^- groups. This is probably a good model for the observed LBHB in HCA II, in which the deep water is in a hydrophobic environment and likely involves the zinc-bound hydroxide.

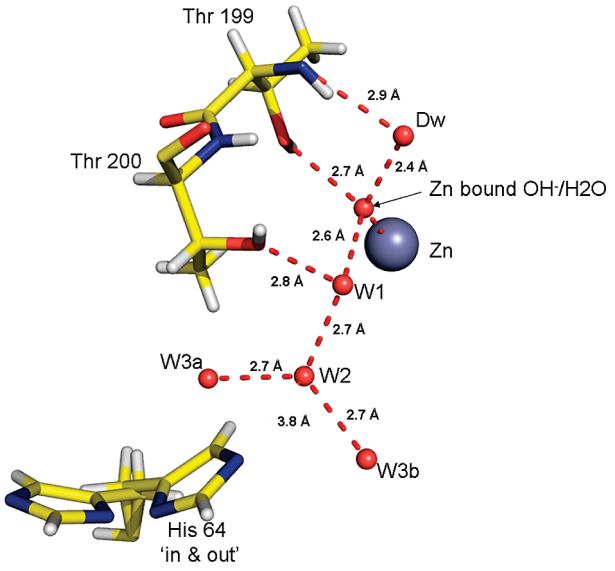

FIGURE 3: Ordered water network in the active site of HCA II. The zinc is represented by a gray sphere, and the oxygen atoms of water molecules are represented as smaller red spheres. Dotted lines are presumed hydrogen bonds with heavy atom distances given. Stick figures are selected amino acids of the active site with both the inward and outward orientations of His64 shown. This figure was created using PyMOL (*28*).

Weak hydrogen bonds typical of water molecules in solution have a favorable enthalpy of formation near 5 kcal/mol; however, LBHBs can have such enthalpies near 15−25 kcal/mol (*13*). This is significant with respect to the catalysis by HCA II since the binding of CO_2 to its catalytically productive binding site displaces the deep water molecule (Dw) (Figure 2) (*16*, *17*) and thus requires the cleavage of the LBHB contributing to the very weak binding of CO_2 at this site. A dissociation constant for CO_2 at its catalytic site in HCA II has been estimated to be 100 mM measured by infrared spectroscopy (*18*, *19*).

A tight binding of substrate at the reactive site is a disadvantage for catalysis by HCA II; it adversely affects its physiological function which requires it to enhance catalysis for a maximum velocity k_{cat} of 10^6 s^{-1} and near diffusion-controlled second-order rate constants for hydration. In arguments elucidated by Fersht (*20*), the tight binding of substrate (without affecting the transition state) lowers the energy level of the substrate−enzyme complex, thereby increasing the activation energy of k_{cat}. When a thermodynamic well or pit that accumulates tightly bound substrate exists, the rate of catalysis is decreased. For an enzyme that requires rapid catalysis like carbonic anhydrase, it is advantageous for substrate binding to be weak and the active site to remain largely unbound at physiological levels of substrate CO_2. The concentration of CO_2 in plasma, for example, is near 1 mM; the value of K_m for hydration is 10 mM, and the estimated dissociation constant of CO_2 is 100 mM. It appears that HCA II evolved weak substrate binding by having it displace the Dw which participates in a LBHB.

There is likely another role for the LBHB as it may contribute to the low pK_a near 7 for the zinc-bound water molecule, the protolysis of which is enhanced using the energy of formation of the LBHB. In this respect, the role of the LBHB is analogous with the catalytic mechanism of liver alcohol dehydrogenase in which removal of a proton from the Zn-coordinated alcohol is promoted by formation of a LBHB with Ser48 in the reactant state (*21*). The alkoxide then undergoes hydride transfer to

generate product. In each case, forming the LBHB provides the energy to pump the proton to His64 in HCA II and to His51 in horse liver alcohol dehydrogenase (*21*).

It is unclear whether these arguments will apply in the dehydration direction in which the maximal catalytic rates are slower than in hydration [maximal steady-state constants are $k_{cat}/K_m = 2 \times 10^7\ M^{-1}\ s^{-1}$ and $k_{cat} = 0.6\ \mu s^{-1}$ (*22*)]. Crystal structures of bicarbonate bound at the active site metal, the presumed catalytic site, have been obtained for the mutant of HCA II with Thr200 replaced with His (*23*), with Thr199 replaced with Ala (*24*), and for HCA II in which Zn(II) is replaced with Co(II) (*25*). Although the orientation of the bound bicarbonate is somewhat different in each of these examples, in all three cases the binding of bicarbonate displaces the deep water. The dissociation constant of bicarbonate at the active site of HCA II is estimated to be ~100 mM by ^{13}C NMR measurements (*26*), with a similar K_i value estimated by inhibition by bicarbonate of the esterase capacity of HCA II (*27*). The value of K_m for dehydration is 32 mM (*22*), and the concentration of bicarbonate in plasma is ~24 mM. However, the form of the enzyme that is catalytic in the dehydration direction contains zinc-bound water. This configuration is not comparable to a hydrated hydroxide, and a LBHB will likely not be found in this case. Hence, at present, we cannot make the argument that weak binding of bicarbonate is caused in part by the displacement of the deep water which participates in a LBHB.

This effect of the LBHB in catalysis to weaken substrate binding in HCA II is different from the effect shown in examples for which the formation of a LBHB not in the enzyme−substrate complex but in the transition state lowers the overall free energy of activation (*13*).

ACKNOWLEDGMENT

We thank Professor W. Wallace Cleland for helpful comments.

SUPPORTING INFORMATION AVAILABLE

Materials and methods, a table of refinement statistics for the structure of human carbonic anhydrase II, a figure of bond lengths in the active site, and a figure of bond angles in the active site. This material is available free of charge via the Internet at http://pubs.acs.org.

REFERENCES

1. Lindskog, S. (1997) *Pharmacol. Ther. 74*, 1–20.
2. Silverman, D. N., and McKenna, R. (2007) *Acc. Chem. Res. 40*, 669–675.
3. Liljas, A., Lovgren, S., Bergsten, P. C., Carlbom, U., Petef, M., Waara, I., Strandbe, B., Fridborg, K., Jarup, L., and Kannan, K. K. (1972) *Nat. New Biol. 235*, 131–137.
4. Nair, S. K., and Christianson, D. W. (1991) *J. Am. Chem. Soc. 113*, 9455–9458.
5. Fisher, S. Z., Maupin, C. M., Budayova-Spano, M., Govindasamy, L., Tu, C., Agbandje-McKenna, M., Silverman, D. N., Voth, G. A., and McKenna, R. (2007) *Biochemistry 46*, 2930–2937.
6. Christianson, D. W., and Fierke, C. A. (1996) *Acc. Chem. Res. 29*, 331–339.
7. Maupin, C. M., McKenna, R., Silverman, D. N., and Voth, G. A. (2009) *J. Am. Chem. Soc. 131*, 7598–7608.
8. Roy, A., and Taraphder, S. (2007) *J. Phys. Chem. B 111*, 10563–10576.
9. Riccardi, D., Konig, P., Guo, H., and Cui, Q. (2008) *Biochemistry 47*, 2369–2378.
10. Cui, Q., and Karplus, M. (2003) *J. Phys. Chem. B 107*, 1071–1078.
11. Smedarchina, Z., Siebrand, W., Fernandez-Ramos, A., and Cui, Q. (2003) *J. Am. Chem. Soc. 125*, 243–251.
12. Fisher, S. Z., Tu, C. K., Bhatt, D., Govindasamy, L., Agbandje-McKenna, M., McKenna, R., and Silverman, D. N. (2007) *Biochemistry 46*, 3803–3813.
13. Cleland, W. W. (2000) *Biochemistry 39*, 1580–1580.
14. Avvaru, B. S., Arenas, D. J., Tu, C. K., Tanner, D. B., McKenna, R., and Silverman, D. N. (2009) *Biochemistry*, submitted for publication.
15. Abudari, K., Raymond, K. N., and Freyberg, D. P. (1979) *J. Am. Chem. Soc. 101*, 3688–3689.
16. Domsic, J. F., Avvaru, B. S., Kim, C. U., Gruner, S. M., Agbandje-McKenna, M., Silverman, D. N., and Mckenna, R. (2008) *J. Biol. Chem. 283*, 30766–30771.
17. Sjoblom, B., Polentarutti, M., and Djinovic-Carugo, K. (2009) *Proc. Natl. Acad. Sci. U.S.A. 106*, 10609–10613.
18. Krebs, J. F., Rana, F., Dluhy, R. A., and Fierke, C. A. (1993) *Biochemistry 32*, 4496–4505.
19. Riepe, M. E., and Wang, J. H. (1968) *J. Biol. Chem. 243*, 2779.
20. Fersht, A. (1999) Structure and Mechanism in Protein Science, W. H. Freeman & Co., New York.
21. Ramaswamy, S., Park, D. H., and Plapp, B. V. (1999) *Biochemistry 38*, 13951–13959.
22. Steiner, H., Jonsson, B. H., and Lindskog, S. (1975) *Eur. J. Biochem. 59*, 253–259.
23. Xue, Y. F., Vidgren, J., Svensson, L. A., Liljas, A., Jonsson, B. H., and Lindskog, S. (1993) *Proteins: Struct., Funct., Genet. 15*, 80–87.
24. Xue, Y. F., Liljas, A., Jonsson, B. H., and Lindskog, S. (1993) *Proteins: Struct., Funct., Genet. 17*, 93–106.
25. Hakansson, K., and Wehnert, A. (1992) *J. Mol. Biol. 228*, 1212–1218.
26. Simonsson, I., Jonsson, B. H., and Lindskog, S. (1979) *Eur. J. Biochem. 93*, 409–417.
27. Steiner, H., Jonsson, B. H., and Lindskog, S. (1976) *FEBS Lett. 62*, 16–20.
28. DeLano, W. L. (2008) The PyMOL Molecular Graphics System, DeLano Scientific LLC, Palo Alto, CA.

Supporting Information

A Short, Strong Hydrogen Bond in the Active Site of Human Carbonic Anhydrase II

Balendu Sankara Avvaru,[a] Chae Un Kim[b], Katherine H. Sippel,[a] Sol M. Gruner[b,c], Mavis Agbandje-McKenna[a], David N. Silverman[a,d,*], Robert McKenna[a,*]

Department of Biochemistry and Molecular Biology[a], Department of Pharmacology and Therapeutics[d], College of Medicine, University of Florida, Gainesville, Florida 32610, USA and Cornell High Energy Synchrotron Source (CHESS)[b], Physics Department[c], Cornell University, Ithaca, NY 14853, USA.

[*]Corresponding authors: D.N.S. Department of Pharmacology, College of Medicine, University of Florida, Box 100267, Gainesville, Florida 32610; Phone: (352) 392 3556; Fax (352) 392 9696; e-mail: silvrmn@ ufl.edu; R.M. Department of Biochemistry and Molecular Biology, College of Medicine, University of Florida, Box 100245, Gainesville, Florida 32610; Phone: 352-392-5696; Fax: 352-392-3422; e-mail: rmckenna@ufl.edu.

Materials and methods

Expression and Purification of HCA II. The plasmid encoding HCA II was transformed into E.coli BL21 cells through standard procedures and the transformed cells were expressed at 37 ºC in LB medium containing 100 μg/ml ampicillin (*1*). HCA II production was induced by the addition of isopropyl thiogalactoside to a final concentration of 1mM at an $O.D_{600}$ of 0.6 AU. The cells were harvested 4 hrs after induction. The cell pellets were lysed and HCA II was purified through affinity chromatography using pAMBS resin as has been described elsewhere (*2*).

Crystallization and X-ray data collection of HCA II. Crystals of HCA II were obtained using the hanging drop vapor diffusion method (*3)*. Ten μl drops of equal amounts of protein and precipitant were equilibrated against precipitant solution (1.3 M sodium citrate; 50mM Tris-HCl; pH 7.0) at room temperature (~20 ºC) (*4)*. A crystal was cryoprotected by quick immersion into 20% glycerol precipitant solution and flash-cooled by exposing it to a gaseous stream of nitrogen at 100K. X-ray diffraction data were collected at the Cornell High Energy Synchrotron Source (CHESS) F1 Station with the wavelength of 0.9173 Å. Quantum 270 was used and the distance was 100 mm to allow 1 degree oscillation without spot overlapping. To cover high resolution spots, the detector was offset (moved upwards). Indexing, integration, and scaling were performed using HKL2000 (*5)*.

Structure determination of HCA II. The crystal structure of HCA II (PDB accession code: 2ILI) (*4)* was used to obtain initial phases of the apo-structure using SHELX97 (*6)*. The zinc and all solvent molecules were removed to avoid model bias. 5% of the unique reflections were selected randomly and excluded from the refinement

data set for the purpose of R_{free} calculations (*7)*. Structural refinement proceeded using SHELXL initially with data from 50.0 to 2.0 Å resolution. The protein geometry was defined using the default constrains of conjugate-least squares (CGLS) mode in SHELXL. Each round of CGLS comprised of 15 cycles of refinement. $2F_o–F_c$ and $F_o–F_c$ electron density Fourier difference maps were calculated after each successive round of CGLS and manually inspected by the graphics program COOT (*8)* for further fine-tuning of the model and the incorporation of solvent molecules. After some initial rounds of CGLS refinement, the resolution was extended to 0.9 Å and subsequently after several more cycles of refinement, the model was further subjected to several cycles of full anisotropic refinement and hydrogen riding which led a convergence of R_{cryst} and R_{free} to 12.5 and 13.1, respectively. The geometry of the final model was checked using the PROCHECK algorithm (*9)*. The RMSD for bond lengths and bond angles were found to be within accepted limits of 0.004 Å and 1.0°, respectively. It was observed that 89 % of the dihedral angles were in the most favored region while the rest were in the allowed region with the exception of 0.5 % which were in the generously allowed region. The geometry and statistics of the final model are summarized in Table S1.

Table S1. Refinement and model statistics for HCA II

Unit cell dimensions, *a, b, c* (Å), β (°)	42.2,41.3,72.2,104.2
Resolution (Å)	50 – 0.9 (0.92-0.9)
Number of unique Reflections	164840 (6751)
Completeness (%)	92.3(76.1)
Redundancy	6.1 (2.8)
R_{symm}[a] I/σ(I)	7.8 (58.0) 25.0 (2.0)
R_{cryst}[b] /R_{free}[c]	12.5 / 13.1
Ramachandran statistics (%) Most favored, additionally allowed and generously allowed regions	89.0, 10.5, 0.5
Number of protein/solvent atoms	2327/487
Average B factors(Å^2) main/side chain Zn/solvent	 10.9/15.2 6.5/26.0

Values in parentheses refer to the highest resolution bin. [a] $R_{symm} = \Sigma |I - \langle I \rangle| / \Sigma \langle I \rangle \times 100$. [b] $R_{cryst} = \Sigma ||Fo| - |Fc|| / \Sigma |F_{obs}| \times 100$. [c] R_{free} is calculated in same manner as R_{cryst}, except that it uses 5% of the reflection data omitted from refinement.

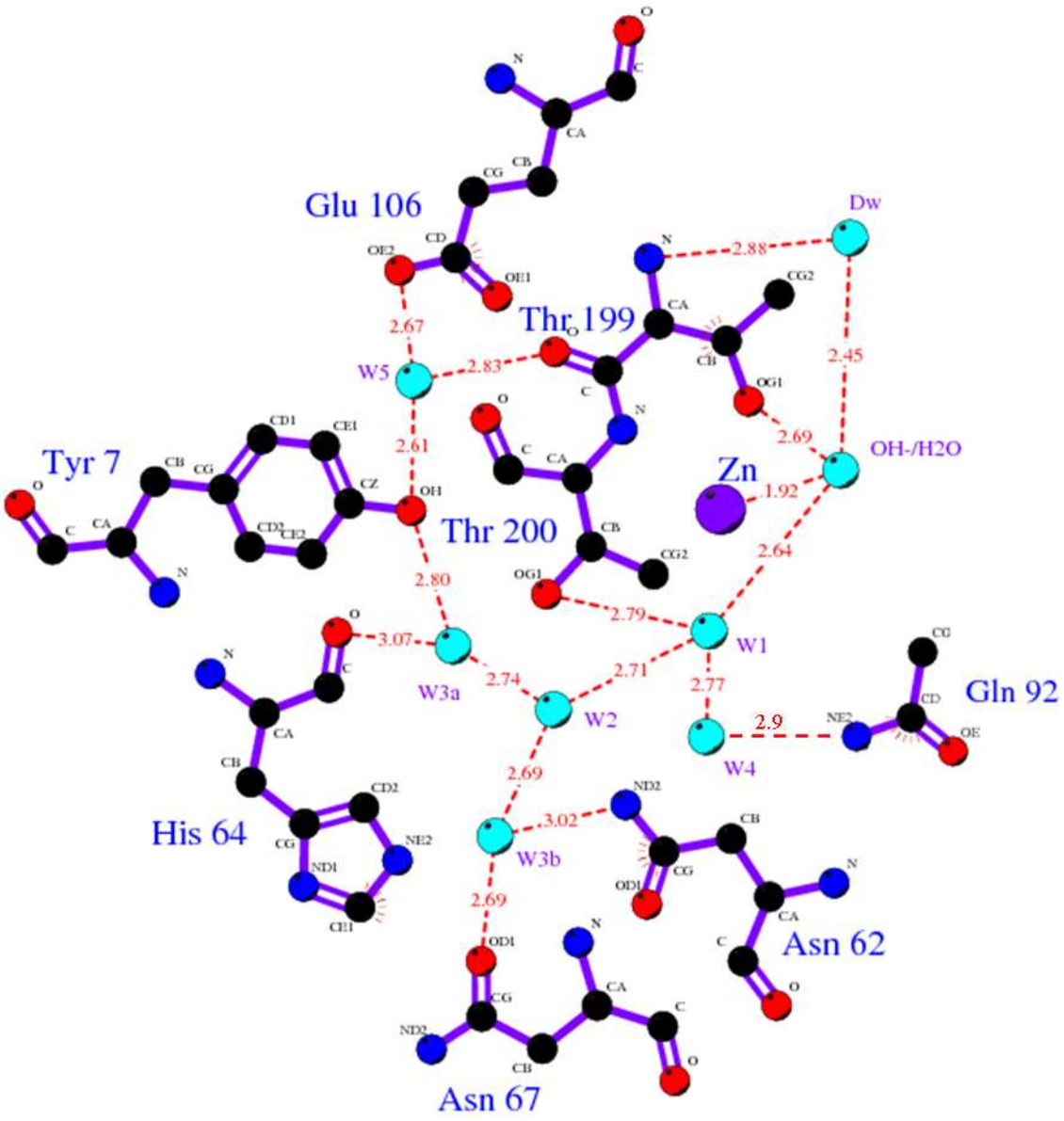

Figure S1. Two dimensional representation of Figure 1. Bond lengths of the oxygen atoms in their respective hydrogen bonding partners are given. Note: The figure is not to scale. Figure created using Ligplot.

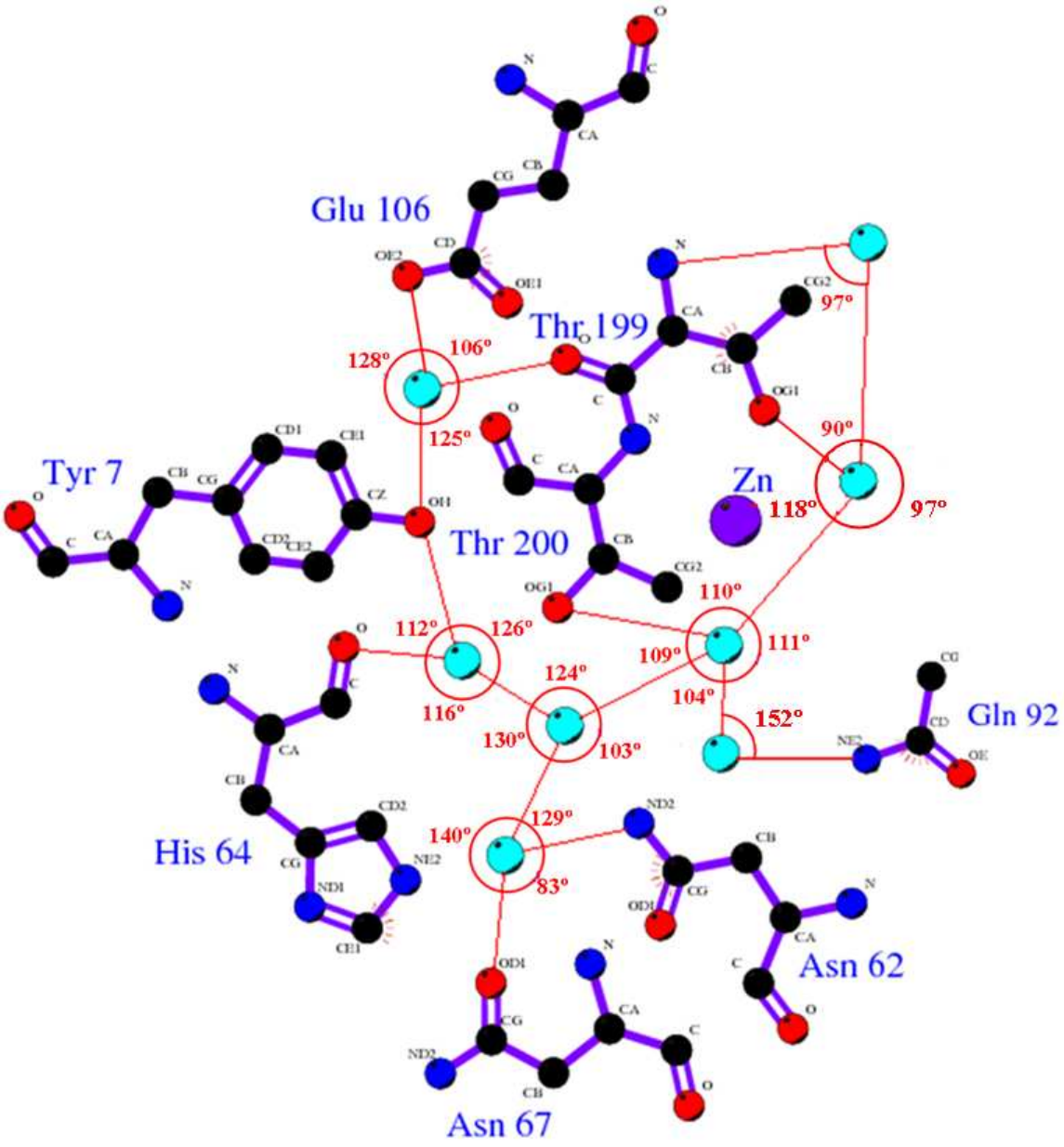

Figure S2. Two dimensional representation of Figure 1. Bond angles of the oxygen atoms to their respective hydrogen bonding partners are given. Note: The figure is not to scale. Figure created using Ligplot.

References

1. Forsman, C. A., Behravan, G., Osterman, A., and Jonsson, B. H. (1988) Production of active human carbonic anhydrase II in E. coli, *Acta. Chem. Scand.* 42, 314–318.
2. Khalifah, R. G., Strader, D. J., Bryant, S. H., and Gibson, S. M. (1977) Carbon-13 nuclear magnetic resonance probe of activesite ionizations in human carbonic anhydrase, *Biochemistry* 16, 2241–2247.
3. McPherson, A. (1982) Preparation and Analysis of Protein Crystals, 1st Ed., Wiley, New York.
4. Fisher, S. Z., C. M. Maupin,M. Budayova-Spano, L. Govindasamy,C. K. Tu, M. Agbandje-McKenna,D. N. Silverman,G. A. Voth, R. McKenna. (2007) Atomic Crystal and Molecular Dynamics Simulation Structures of Human Carbonic Anhydrase II: Insights into the Proton Transfer Mechanism, *Biochemistry* 46, 2930-2937.
5. Otwinowski, Z., and Minor, W. (1997) Processing of x-ray diffraction data collected in oscillation mode, *Methods Enzymol.* 276, 307–326.
6. Sheldrick, G. M. (2008) A Short History of SHELX. *Acta Crystallogr. Sect. A* 64, 112–122.
7. Brunger, A. T. (1992) Free R value: A novel statistical quantity for assessing the accuracy of crystal structures, *Nature* 355, 472–475.
8. Emsley, P., and Cowtan, K. (2004) Coot: model-building tools for molecular graphics, *Acta Crystallogr. Sect. D* 60, 2126–2132
9. Laskowski, R. A., MacArthur, M. W., Moss, D. S., and Thornton, J. M. (1993) PROCHECK: a program to check the stereochemical quality of protein structures, *J. Appl. Cryst.* 26, 283–291.